

# Selective field evaporation in field-ion microscopy for ordered alloys

Xi-jin Ge<sup>a)</sup>

*Institute of Applied Physics, Beijing University of Science and Technology, Beijing 100083, China and Research into Artifacts, Center for Engineering (RACE), University of Tokyo, 4-6-1 Komaba, Meguro-ku, Tokyo 153-8904, Japan*

Nan-xian Chen

*Institute of Applied Physics, Beijing University of Science and Technology, Beijing 100083, China and CCAST (World Laboratory), P.O. Box 8730, Beijing 100080, China*

Wen-qing Zhang<sup>b)</sup>

*Institute of Applied Physics, Beijing University of Science and Technology, Beijing 100083, China*

Feng-wu Zhu

*Department of Materials Physics, Beijing University of Science and Technology, Beijing 100083, China*

(Received 22 May 1998; accepted for publication 19 December 1998)

Semiempirical pair potentials, obtained by applying the Chen-inversion technique to a cohesion equation of Rose *et al.* [Phys. Rev. B **29**, 2963 (1984)], are employed to assess the bonding energies of surface atoms of intermetallic compounds. This provides a new calculational model of selective field evaporation in field-ion microscopy (FIM). Based on this model, a successful interpretation of FIM image contrasts for Fe<sub>3</sub>Al, PtCo, Pt<sub>3</sub>Co, Ni<sub>4</sub>Mo, Ni<sub>3</sub>Al, and Ni<sub>3</sub>Fe is given. © 1999 American Institute of Physics. [S0021-8979(99)07306-5]

## I. INTRODUCTION

There are perfect ring structures in the field-ion microscopy (FIM) images of pure metals. The prominent poles in these images correspond to the crystallographic planes of high atomic density. For ordered alloys similar ring structures are also observed. In the FIM image of an ordered binary alloy, usually one atomic species is bright whereas the other is dim, or even invisible.<sup>1-3</sup> It is found that the invisible species are Co in Pt-Co alloys,<sup>4-6</sup> Ni in D1<sub>a</sub>-Ni<sub>4</sub>Mo,<sup>7-10</sup> and Fe in D0<sub>3</sub>-Fe<sub>3</sub>Al.<sup>11-14</sup>

This phenomenon can be related to the stability of the respective atomic species towards field evaporation.<sup>15</sup> When voltage pulses are applied during tip preparation, one species will evaporate preferentially with respect to the other (selective field evaporation), thereby being removed from its possible imaging sites. The conventional viewpoint is that the species with the smaller sublimation energy in the pure-metal state evaporates more easily.<sup>1,3,11</sup> This can explain the image contrast in some alloys including Pt-Co and Ni<sub>4</sub>Mo, but gives wrong predictions for Fe<sub>3</sub>Al and Ni<sub>3</sub>Fe. Due to the change in bonding during the formation of an alloy, the field-evaporation stability of atoms in the alloy can barely be evaluated by the sublimation energies of the pure metals.

In this article, interatomic potentials are obtained via inversion from *ab initio* or semiempirical cohesive energy curves. Bonding energies of surface atoms of intermetallic compounds are calculated in order to predict the selective field evaporation behavior. A qualitative interpretation of image contrast for several alloys is presented.

This article is organized as follows. In Sec. II the inversion technique to derive pair potentials is outlined. In the beginning of Sec. III, we perform a direct simulation of a specimen tip by calculating the bonding energies of various kink site (KS) atoms. Then it is shown that the problem can be simplified and the relative stability can be evaluated by the bonding energies of surface atoms. The calculated results for six kinds of ordered alloys are given in Sec. IV. Finally, Sec. V includes discussion and conclusion.

## II. DERIVATION OF PAIR POTENTIALS

The method of obtaining parameter-free pair potentials from *ab initio* total energy calculations was first used by Carlsson, Gelatt, and Ehrenreich (CGE).<sup>16</sup> Chen *et al.*<sup>17-19</sup> improved the method based on the Möbius inversion formula in number theory.<sup>20</sup> Chen's inversion technique has a faster convergence than the CGE method.

According to pair potential approximation, the cohesive energy of a metal can be expressed as

$$E(x) = \frac{1}{2} \sum_{n=1}^{\infty} r_0(n) \phi[b_0(n)x], \quad (1)$$

where  $x$  is the nearest neighbor distance,  $\phi[b_0(n)x]$  the pair potential between two atoms separated by a distance  $b_0(n)x$ , and  $r_0(n)$  the number of  $n$ th nearest neighbor atoms. To solve the pair potential  $\phi(x)$  from Eq. (1), we first extend the series  $\{b_0(n)\}$  to  $\{b(n)\}$  to achieve multiplicative closeness. The closeness ensures that for any positive integers  $m$  and  $n$ , there exists an integer  $k$  satisfying the relation,

$$b(k) = b(m)b(n). \quad (2)$$

Then, Eq. (1) is equivalent to the following:

<sup>a)</sup>Electronic mail: xge@race.u-tokyo.ac.jp

<sup>b)</sup>Present address: Division of Applied Sciences, Harvard University, Cambridge, MA 02138.

TABLE I. Import parameters of the Rose equation for metals and alloys. Units are Å for lattice constants,  $10^{11}$  N/m<sup>2</sup> for bulk modulus, and eV for cohesive energy.

	Structure	Lattice constants (a/c)	Bulk modulus	Cohesive energy
Fe	bcc	2.87	1.683	4.28
Al	fcc	4.05	0.722	3.39
Fe <sub>3</sub> Al	D0 <sub>3</sub>	5.792 <sup>a</sup>	1.441 <sup>c</sup>	4.22 <sup>b</sup>
Pt	fcc	3.92	2.783	5.84
Co	fcc	3.43 <sup>b</sup>	2.910 <sup>b</sup>	6.89 <sup>b</sup>
Pt <sub>3</sub> Co	L1 <sub>2</sub>	3.84 <sup>a</sup>	2.61 <sup>b</sup>	5.51 <sup>b</sup>
PtCo	L1 <sub>0</sub>	3.812/3.708 <sup>a</sup>		
Ni	fcc	3.52	1.860	4.44
Mo	bcc	3.15	2.725	6.82
Ni <sub>3</sub> Mo	L1 <sub>2</sub>	3.58 <sup>a</sup>	2.51 <sup>b</sup>	5.67 <sup>b</sup>
Ni <sub>4</sub> Mo	D1 <sub>a</sub>	5.720/3.564 <sup>a</sup>		
Ni <sub>3</sub> Al	L1 <sub>2</sub>	3.567 <sup>a</sup>	1.86 <sup>c</sup>	4.57 <sup>b</sup>
Ni <sub>3</sub> Fe	L1 <sub>2</sub>	3.552 <sup>b</sup>	2.66 <sup>b</sup>	4.50 <sup>b</sup>

<sup>a</sup>Reference 22.

<sup>b</sup>LAPW calculation in this work.

<sup>c</sup>Reference 23; other data from Ref. 24.

$$E(x) = \frac{1}{2} \sum_{n=1}^{\infty} r(n) \phi[b(n)x], \quad (3)$$

where

$$r(n) = \begin{cases} r_0(b_0^{-1}[b(n)]), & \text{if } b(n) \in \{b_0(n)\}; \\ 0, & \text{if } b(n) \notin \{b_0(n)\}. \end{cases} \quad (4)$$

The lattice point is said to be virtual when  $r(n)=0$ . The solution to Eq. (3) is given by

$$\phi(x) = 2 \sum_{n=1}^{\infty} I(n) E[b(n)x], \quad (5)$$

where the inversion coefficient  $I(n)$  is determined by

$$\sum_{b(n)|b(k)} I(n) r \left[ b^{-1} \left( \frac{b(k)}{b(n)} \right) \right] = \delta_{k1}. \quad (6)$$

Hence, if  $E(x)$  is known, the pair potential  $\phi(x)$  can be obtained from Eq. (5). For  $E(x)$ , we use the universal cohesion equation of Rose *et al.*,<sup>21</sup> namely,

$$E(x) = E_0(1+x^*)e^{-x^*}, \quad (7)$$

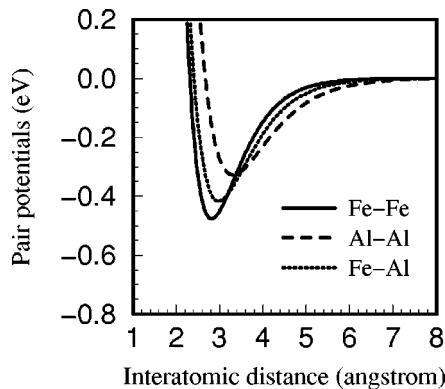


FIG. 1. Pair potentials  $\phi_{\text{Fe-Fe}}(x)$ ,  $\phi_{\text{Al-Al}}(x)$ , and  $\phi_{\text{Fe-Al}}(x)$ .

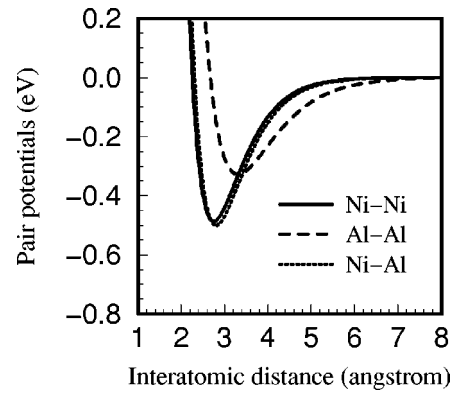


FIG. 2. Pair potentials  $\phi_{\text{Ni-Ni}}(x)$ ,  $\phi_{\text{Al-Al}}(x)$ , and  $\phi_{\text{Ni-Al}}(x)$ .

with

$$x^* = \sqrt{\frac{9B\Omega}{E_0}} \left( \frac{x}{x_0} - 1 \right),$$

where  $\Omega$  and  $x_0$  are the equilibrium atomic volume and nearest neighbor distance,  $E_0$  the sublimation energy, and  $B$  the bulk modulus. The parameters ( $x_0$ ,  $E_0$ , and  $B$ ) for the present work are given in Table I, where experimental data are used if available. The unavailable data of some alloys are calculated from first principles through the following steps. First, the cohesive energies of an alloy with different lattice constants are calculated using the linearized augmented plane-wave (LAPW) method.<sup>25,26</sup> These data are then fitted to the Rose equation to obtain the parameters  $x_0$ ,  $E_0$ , and  $B$ . It is found that the calculated data can be well fitted to the Rose equation.

From the cohesion equations of metals, the pair potentials between identical atoms (Fe-Fe, Al-Al, etc.) can be directly obtained by using Eq. (5). For the pair potentials between unlike atoms (Fe-Al, Ni-Al, etc.) we use *partial cohesive energy curves* of intermetallic compounds.<sup>23</sup> For example, in the case of Fe<sub>3</sub>Al, a partial cohesive energy curve  $E_{\text{Fe-Al}}(x)$  is calculated by subtracting the Fe-Fe and Al-Al interactions from the cohesion equation of D0<sub>3</sub>-Fe<sub>3</sub>Al. Because  $E_{\text{Fe-Al}}(x)$  can be written as the summation of  $\phi_{\text{Fe-Al}}(x)$  in the form of Eq. (1), the formal solution to Eq. (1) given by Eq. (5) is applicable to compute  $\phi_{\text{Fe-Al}}(x)$

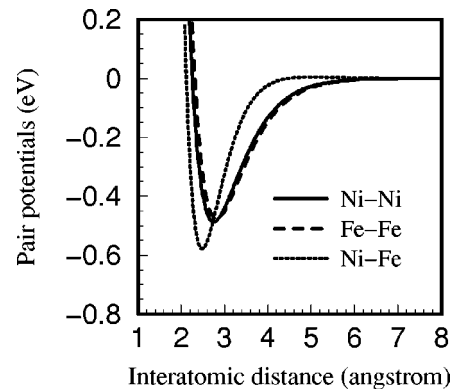
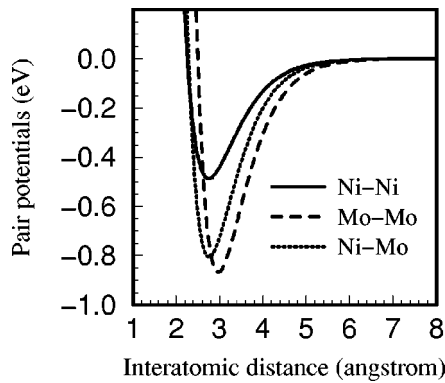
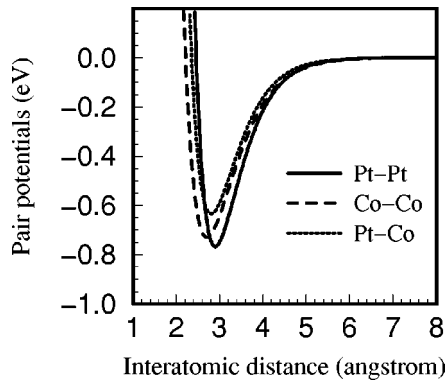
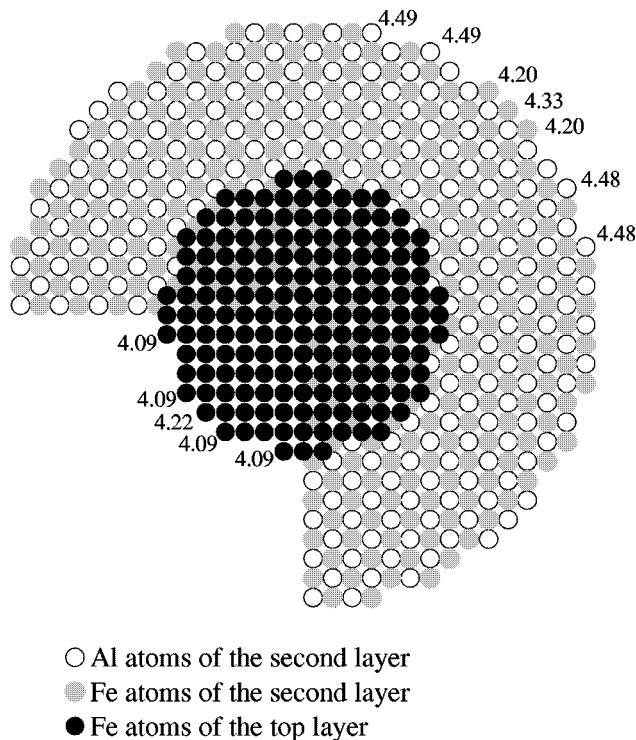


FIG. 3. Pair potentials  $\phi_{\text{Ni-Ni}}(x)$ ,  $\phi_{\text{Fe-Fe}}(x)$ , and  $\phi_{\text{Ni-Fe}}(x)$ .

FIG. 4. Pair potentials  $\phi_{\text{Ni-Ni}}(x)$ ,  $\phi_{\text{Mo-Mo}}(x)$ , and  $\phi_{\text{Ni-Mo}}(x)$ .FIG. 5. Pair potentials  $\phi_{\text{Pt-Pt}}(x)$ ,  $\phi_{\text{Co-Co}}(x)$ , and  $\phi_{\text{Pt-Co}}(x)$ .

○ Al atoms of the second layer  
 ◐ Fe atoms of the second layer  
 ● Fe atoms of the top layer

FIG. 6. A top view of the atomic arrangement of the first and second layer of a  $\langle 001 \rangle$  pole of a  $\text{D0}_3\text{-Fe}_3\text{Al}$  FIM tip. The radius of curvature is 500 Å. The number next to a kink site atom denotes the bonding energies (in eV) of the atom. Note that one fourth of the second layer is not shown in order to make the top layer clear.

TABLE II. Calculated bonding energies (in eV) of surface and bulk atoms in  $\text{D0}_3\text{-Fe}_3\text{Al}$ . The coordinates of atoms in the unit cell in the second column should be repeated by adding  $(0, 1/2, 1/2)$ ,  $(1/2, 0, 1/2)$ , and  $(1/2, 1/2, 0)$ , respectively.

	Coordinates	(100)	(110)	(111)	(210)	Bulk
Fe	(3/4, 1/4, 1/4)	5.319	5.380	4.316	4.576	8.185
Fe	(1/4, 1/4, 1/4)	5.319	5.380	4.647	4.576	8.185
Fe	(1/2, 0, 0)	5.321	5.617	4.594	4.630	8.409
Al	(0, 0, 0)	5.821	5.722	5.144	5.946	8.971

from  $E_{\text{Fe-Al}}(x)$ . That is to say, pair potentials between unlike atoms can be derived from cohesive energy curves of alloys.

Figure 1 shows the pair potentials for the simulation of  $\text{Fe}_3\text{Al}$ , namely,  $\phi_{\text{Fe-Fe}}(x)$ ,  $\phi_{\text{Fe-Al}}(x)$ , and  $\phi_{\text{Al-Al}}(x)$ . Similarly, Figs. 2 and 3 are potential functions for  $\text{Ni}_3\text{Al}$  and  $\text{Ni}_3\text{Fe}$ . Since it is difficult to perform LAPW calculations for  $\text{D1}_a\text{-Ni}_4\text{Mo}$ , we calculate the cohesive energy curve of  $\text{Ni}_3\text{Mo}$  with  $\text{L1}_2$  structure and derive  $\phi_{\text{Ni-Mo}}(x)$  from it (Fig. 4). It is assumed that the potential is transferable to  $\text{Ni}_4\text{Mo}$ . As the hcp structure of Co with  $c/a = 1.6215$  is inconvenient for inversion,  $\phi_{\text{Co-Co}}(x)$  is derived from the calculated cohesive energy curve of fcc Co. The pair potential  $\phi_{\text{Pt-Co}}(x)$  (Fig. 5) is obtained from the partial cohesive energy curve of  $\text{L1}_2\text{-Pt}_3\text{Co}$ .

### III. CALCULATION OF BONDING ENERGIES

The tip of a FIM specimen is nearly hemispherical with a radius of curvature of about 500–1000 Å. As an example, Fig. 6 shows one possible atomistic configuration of the two top layers of a  $\langle 001 \rangle$  pole of  $\text{D0}_3\text{-Fe}_3\text{Al}$ . The radius of curvature is assumed to be 500 Å. The first layer contains only Fe atoms and the second layer contains both Fe and Al atoms. Since field evaporation occurs exclusively from kink sites (KSs), the relative stability of atomic species can be determined by the bonding energies of different atoms at the KSs. The bonding energy of the  $i$ th KS atom is defined as the sum of pair potentials between the  $i$ th atom and the other atoms on the tip, namely

$$E_i^t = \sum_{j \neq i, j \in \text{tip}} \phi_{ij}(r_{ij}). \quad (8)$$

The calculated bonding energies of some KS atoms are also provided in Fig. 6. The bonding energy of an Fe KS atom is about 4.10 eV in the pure layer and 4.20 eV in the mixed layer, while Al KS atoms have higher bonding energies of about 4.50 eV. Therefore, Fe atoms tend to evaporate pref-

TABLE III. Calculated bonding energies (in eV) of surface and bulk atoms in  $\text{D1}_a\text{-Ni}_4\text{Mo}$ . The coordinates of atoms in the unit cell in the second column should be repeated by adding  $(1/2, 1/2, 1/2)$ .

	Coordinates	(100)	(001)	(110)	(111)	Bulk
Ni	(0.2, 0.4, 0)	5.014	6.560	5.200	4.791	9.900
Ni	(0.6, 0.2, 0)	5.211	6.560	4.008	4.914	9.900
Ni	(0.4, 0.8, 0)	5.199	6.560	5.666	4.987	9.900
Ni	(0.8, 0.6, 0)	5.396	6.560	5.474	5.110	9.900
Mo	(0, 0, 0)	7.856	9.517	8.164	7.276	14.553

TABLE IV. Calculated bonding energies (in eV) of surface and bulk atoms in L1<sub>2</sub>-Pt<sub>3</sub>Co and L1<sub>0</sub>-PtCo.

PtCo(L1 <sub>0</sub> )	Coordinates	(100)	(110)	(111)	(210)	bulk
Co	(0,0,0),(1/2,1/2,0)	4.695	4.762	5.138	4.070	7.494
Pt	(0,1/2,1/2),(1/2,0,1/2)	6.093	6.350	5.329	4.974	9.694
Pt <sub>3</sub> Co(L1 <sub>2</sub> )	Coordinates	(100)	(110)	(111)	(210)	bulk
Co	(0,0,0)	4.365	3.921	4.517	3.561	6.589
Pt	(0,1/2,1/2)	7.568	7.639	8.730	6.665	12.494
Pt	(1/2,1/2,0)	8.789	6.999	8.730	6.665	12.494
Pt	(1/2,0,1/2)	8.789	7.639	8.730	6.635	12.494

erentially and hence are invisible in the FIM image of D0<sub>3</sub>-Fe<sub>3</sub>Al. This is in agreement with experiments.<sup>11-14</sup>

Figure 6 is only one possible atomic arrangement of the two top layers. There are numerous KS atoms on the lower layers, which are impossible to describe explicitly. Moreover, the detailed shape of a specimen tip is complicated and is not fully taken into account by our simple model. Therefore it is necessary to introduce a parameter to depict the bonding-energy difference between two species of KS atoms. As a <hkl> pole is formed by a series of (hkl) planes intercepted by the tip envelope, it is reasonable to assess the difference by calculating the bonding energies of atoms on an ideal (hkl) surface. For example, in order to depict the bonding-energy difference between Fe and Al KS atoms at Fe<sub>3</sub>Al <001> pole, we can calculate the bonding energies of Fe and Al on an ideal (001) surface. An ideal surface means a plane cut along a perfect crystal lattice. The bonding energy of the *i*th atom on the surface is defined by

$$E_i^s = \sum_{j \neq i, j \in \text{surf}} \phi_{ij}(r_{ij}), \tag{9}$$

where the summation is over all the other atoms. If the atoms of one species have larger *E<sup>s</sup>* than those of the other, these atoms will evaporate less easily from the tip surface.

In fact, the bonding-energy difference between atomic species on a surface is a manifestation of the bonding-energy difference within the crystal bulk. The bonding energy of a bulk atom is defined by

$$E_i^b = \sum_{j \neq i, j \in \text{bulk}} \phi_{ij}(r_{ij}), \tag{10}$$

where the summation is over all neighboring atoms in the crystal bulk. The value of *E<sup>b</sup>* can be considered as the energy required to remove an atom from its interior site to infinity. In a metal, all atoms have the same *E<sup>b</sup>*, which is twice the cohesive energy of the metal. However, nonequivalent atoms

in an alloy have different *E<sup>b</sup>*, whose composition-weighted average gives twice the cohesive energy of the alloy. A larger *E<sup>b</sup>* means a stronger bonding between the atom and its neighbors. Generally speaking, atoms with larger *E<sup>b</sup>* also have larger *E<sup>s</sup>* on surfaces. In the following section, we present the calculated results of both *E<sup>s</sup>* and *E<sup>b</sup>*.

#### IV. RESULTS

##### A. Fe<sub>3</sub>Al

The results for D0<sub>3</sub>-Fe<sub>3</sub>Al are given in Table II. Although the sublimation energy of aluminum is smaller than that of iron, the bonding energy *E<sup>b</sup>* of Al atoms in D0<sub>3</sub>-Fe<sub>3</sub>Al is larger than that of Fe atoms. We find that this is caused by the interaction with the third nearest neighbors. All of the third nearest neighbors of an Al atom in Fe<sub>3</sub>Al are Al atoms, while at the corresponding distance  $\phi_{\text{Al-Al}}$  is significantly larger than  $\phi_{\text{Fe-Fe}}$  and  $\phi_{\text{Fe-Al}}$ .

On all the surfaces considered, the bonding energies *E<sup>s</sup>* of Al atoms are approximately 0.1–0.5 eV higher than those of Fe atoms. Consequently, Fe atoms will be removed selectively from the tip surface and become invisible. This agrees with the experimental observation.<sup>11-14</sup>

##### B. Ni<sub>4</sub>Mo

According to the results for D1<sub>a</sub>-Ni<sub>4</sub>Mo in Table III, the *E<sup>b</sup>* of a Mo atom (14.55 eV) is much larger than that of a Ni atom (9.90 eV). On all the surfaces considered, the bonding energies of Mo atoms are also 2 to 3 eV larger than those of Ni atoms. As a result, Ni atoms will evaporate at a much lower electric field, which is consistent with experiments.<sup>7-10</sup>

##### C. Pt-Co

The results for L1<sub>0</sub>-PtCo and L1<sub>2</sub>-Pt<sub>3</sub>Co are given in Table IV. The bonding energies of Pt atoms are larger than

TABLE V. Calculated bonding energies (in eV) of surface and bulk atoms in L1<sub>2</sub>-Ni<sub>3</sub>Al.

	Coordinates	(100)	(110)	(111)	(210)	Bulk
Al	(0,0,0)	6.608	6.007	6.666	5.516	10.042
Ni	(0,1/2,1/2)	5.754	5.259	5.945	4.816	8.837
Ni	(1/2,1/2,0)	5.818	5.248	5.459	4.816	8.837
Ni	(1/2,0,1/2)	5.818	5.259	5.945	4.843	8.837

TABLE VI. Calculated bonding energies (in eV) of surface and bulk atoms in L1<sub>2</sub>-Ni<sub>3</sub>Fe.

	Coordinates	(100)	(110)	(111)	(210)	Bulk
Fe	(0,0,0)	6.470	5.603	6.504	4.980	9.307
Ni	(0,1/2,1/2)	6.223	5.302	5.978	4.940	8.905
Ni	(1/2,1/2,0)	5.791	5.347	5.978	4.940	8.905
Ni	(1/2,0,1/2)	5.791	5.302	5.978	4.975	8.905

TABLE VII. Imaging species obtained by selective field evaporation based on the bonding energies derived by the present work. The table also includes experimental results and predictions from conventional selective field evaporation (based on cohesive energies of metals) and charge transfer (based on the electronegativity).

	D0 <sub>3</sub> -Fe <sub>3</sub> Al	D1 <sub>a</sub> -Ni <sub>4</sub> Mo	L1 <sub>0</sub> -PtCo/L1 <sub>2</sub> Pt <sub>3</sub> Co	L1 <sub>2</sub> -Ni <sub>3</sub> Al	L1 <sub>2</sub> -Ni <sub>3</sub> Fe
Experiment	Al <sup>a</sup>	Mo <sup>b</sup>	Pt <sup>c</sup>	Al <sup>d</sup>	Fe <sup>e</sup>
Conventional selective evaporation	Fe	Mo	Pt	Ni	Ni
Charge transfer	Al	Mo	Co	Al	Fe
Present work	Al	Mo	Pt	Al	Fe

<sup>a</sup>References 11–14.

<sup>b</sup>References 7–10.

<sup>c</sup>References 4–6.

<sup>d</sup>Reference 30.

<sup>e</sup>Reference 29.

those of Co atoms on all the surfaces considered. Accordingly, Co atoms tend to evaporate more easily in both alloys and will be invisible in the FIM image, which agrees with experiments.<sup>4–6</sup>

#### D. Ni<sub>3</sub>Al

The bonding energy of Al bulk atoms in L1<sub>2</sub>-Ni<sub>3</sub>Al is larger than that of Ni atoms by 1.20 eV (see Table V) and the  $E^s$  of Al surface atoms are also larger than those of Ni surface atoms. Thus Al will be the imaging species. This result is in agreement with the experiments by Miller,<sup>27</sup> Brenner and Ming-Jiang.<sup>28</sup>

#### E. Ni<sub>3</sub>Fe

The sublimation energy of nickel is 4.44 eV, which is larger than that of iron (4.28 eV).<sup>24</sup> According to the conventional viewpoint of selective field evaporation,<sup>1,3,11</sup> Ni will be the imaging species in L1<sub>2</sub>-Ni<sub>3</sub>Fe. Nevertheless, our calculation shows that on all the low-index surfaces the bonding energies of Ni atoms are smaller than those of Fe atoms (see Table VI), which leads to the conclusion that Fe atoms will be the bright ones in the FIM image of Ni<sub>3</sub>Fe. Indeed, there is indirect experimental evidence supporting our result. In a FIM image for a  $\langle 100 \rangle$  antiphase boundary of Ni<sub>3</sub>Fe,<sup>29</sup> the clear semi-ring structure indicates that Fe is the imaging species since there are Fe atoms on every other layer and Ni atoms on every layer. If the imaging species is Ni, both semi-parts of each ring would be bright.

### V. DISCUSSION AND CONCLUSION

The mechanism of FIM image formation for ordered alloys has been a well-known experimental puzzle for almost 30 years. In the past, two explanations were proposed, namely the selective field evaporation<sup>4</sup> and the selective ionization<sup>5</sup> (or charge transfer). According to the selective ionization mechanism, since the electrons in a binary alloy transfer from the atomic species of smaller electronegativity to the other one, the local electric field at the sites of the former species is enhanced. Consequently, imaging gas atoms will be preferentially ionized at these sites, and give rise to bright image. However, the present work is based on the viewpoint that the selective field evaporation is the control-

ling factor because it forms the surface structure on the apex of a FIM tip before the occurrence of the selective ionization.<sup>4</sup>

In the present work, the bonding energies of surface atoms of intermetallic compounds are calculated in order to predict qualitatively a selective field evaporation of one atomic species under typical conditions for FIM. It is assumed that atoms with smaller bonding energies will be removed selectively during field evaporation. In Table VII, our predictions are compared with experimental results and predictions made by other models. The table shows that neither conventional selective field evaporation (based on cohesive energies of the metals) nor the charge transfer (based on the electronegativity) can explain all the observations. The selective field evaporation based on bonding energies derived by the present computational method correctly predicts the selective evaporation of Fe, Ni, and Co in FIM tips of Fe<sub>3</sub>Al, Ni<sub>4</sub>Mo, and Pt-Co, respectively. Al atoms are found more stable than Ni atoms on FIM tips of Ni<sub>3</sub>Al, which coincides with most experiments.

The good agreement with experiments can be attributed to the fact that the present calculational model has taken into account the bonding in alloys during the derivation of pair potentials and the calculation of bonding energies of surface atoms. On the other hand, our results indicate that the sublimation energies of metals cannot be used to estimate the bond strength and the field-evaporation stabilities of the corresponding atoms in alloys.

For further study, we might consider some predictions for FIM image contrast for ternary compounds by using this model. A relatively simple model of pair potential has been used in the present work. The many-body effect in the interatomic potentials might have to be taken into account.

### ACKNOWLEDGMENTS

The authors are greatly indebted to Y. Wu, Z. G. Liu, S. Iwata, T. Ashino, Q. Xie, Y. Y. Luo, J. Weng, Y. T. Chang, Y. M. Mi, J. Fu, and Michel Gauthier for their helpful discussions and encouragement. The authors also thank the reviewer of this article for kindly providing detailed advice. One of us, X.J.G., is grateful for a Monbushou scholarship provided by the Japanese government. This work is partly supported by National Advanced Materials Committee of China, and partly by National Science Foundation in China.

- <sup>1</sup>E. W. Müller and T. T. Tsong, *Field Ion Microscopy: Principles and Applications* (Elsevier, New York, 1969).
- <sup>2</sup>R. Wagner, *Field-Ion Microscopy* (Springer, Berlin, 1982).
- <sup>3</sup>M. K. Miller and G. D. W. Smith, *Atom Probe Microanalysis: Principles and Application to Materials Problems* (Materials Research Society, Pittsburgh, 1989).
- <sup>4</sup>H. N. Southworth and B. Ralph, *Philos. Mag.* **14**, 383 (1966).
- <sup>5</sup>T. T. Tsong and E. W. Müller, *J. Appl. Phys.* **38**, 545 (1967); *Appl. Phys. Lett.* **9**, 7 (1966); *J. Appl. Phys.* **38**, 3531 (1967).
- <sup>6</sup>T. T. Tsong, S. V. Krishnaswamy, S. B. Mclane, and E. W. Müller, *Appl. Phys. Lett.* **23**, 1 (1973).
- <sup>7</sup>R. W. Newman and J. J. Hren, *Philos. Mag.* **16**, 211 (1967).
- <sup>8</sup>B. G. LeFevre, H. Grenga, and B. Ralph, *Philos. Mag.* **18**, 1127 (1968).
- <sup>9</sup>M. K. Miller, E. A. Kenik, and T. A. Zagula, *J. Physique* **48-C6**, 385 (1987).
- <sup>10</sup>M. Yamamoto, M. Futamoto, S. Nenno, and S. Nakamura, *J. Phys. Soc. Jpn.* **36**, 1330 (1974).
- <sup>11</sup>J. Weng, F. W. Zhu, and J. M. Xiao, *Z. Metallkd.* **85**, 432 (1994); J. Weng, Ph.D. thesis, Beijing University of Science and Technology, 1995.
- <sup>12</sup>H.-J. Krause-Habrock, G. Frommeyer, J. E. Wittig, and M. Krause, *J. Phys.* **49-C6**, 365 (1988).
- <sup>13</sup>G. Frommeyer, H. J. Habrock, J. E. Wittig, P. Vonczarnowski, J. Geenen, and M. Kreuss, *Scr. Metall. Mater.* **24**, 51 (1990).
- <sup>14</sup>Z. G. Liu, G. Frommeyer, M. Kreuss, J. Wesemann, and N. Wanderka (unpublished).
- <sup>15</sup>H. N. Southworth and B. Ralph, *Philos. Mag.* **21**, 23 (1970).
- <sup>16</sup>A. E. Carlsson, C. D. Gelatt, and H. Ehrenreich, *Philos. Mag. A* **41**, 241 (1980).
- <sup>17</sup>N. X. Chen, *Phys. Rev. Lett.* **64**, 1193 (1990); J. Maddox, *Nature (London)* **344**, 377 (1990).
- <sup>18</sup>N. X. Chen and G. B. Ren, *Phys. Rev. B* **45**, 8177 (1992).
- <sup>19</sup>N. X. Chen, Z. D. Chen, and Y. C. Wei, *Phys. Rev. E* **55**, R5 (1997).
- <sup>20</sup>M. R. Schroeder, *Number Theory in Science and Communication* (Springer, Berlin, 1984).
- <sup>21</sup>J. H. Rose, J. R. Smith, F. Guinea, and J. Ferrante, *Phys. Rev. B* **29**, 2963 (1984).
- <sup>22</sup>W. B. Pearson, *A Handbook of Lattice Spacings and Structures of Metals and Alloys* (Pergamon, London, 1966).
- <sup>23</sup>G. Simmons and H. Wang, *Single Crystal Elastic Constants and Calculated Aggregate Properties* (MIT, Cambridge, 1971).
- <sup>24</sup>C. Kittel, *Introduction to Solid State Physics*, 6th ed. (Wiley, New York, 1986).
- <sup>25</sup>H. Krakauer, M. Posternak, and A. J. Freeman, *Phys. Rev. B* **19**, 1706 (1979).
- <sup>26</sup>W.-Q. Zhang, Q. Xie, X.-J. Ge, and N. X. Chen, *J. Appl. Phys.* **82**, 578 (1997).
- <sup>27</sup>M. K. Miller and J. A. Horton, *Scr. Metall.* **20**, 1125 (1986).
- <sup>28</sup>S. S. Brenner and H. Ming-Jian, *Scr. Metall. Mater.* **25**, 1271 (1991).
- <sup>29</sup>Y. Lin, F. W. Zhu, and J. M. Xiao, *Acta Metall. Mater.* **42**, 2499 (1994).
- <sup>30</sup>This conclusion is drawn from the majority of published results (Refs. 27 and 28) while Hono *et al.* (Ref. 31) found that the imaging species in Ni<sub>3</sub>Al are different in different directions and at different temperatures.
- <sup>31</sup>K. Hono, A. Chiba, T. Sakurai, and S. Hanada, *Acta Metall. Mater.* **40**, 419 (1992).